International Journal of Nanomedicine

Dovepress
open access to scientific and medical research

Open Access Full Text Article

ORIGINAL RESEARCH

Dual-responsive dithio-polydopamine coated porous CeO_2 nanorods for targeted and synergistic drug delivery

This article was published in the following Dove Press journal:
International Journal of Nanomedicine

Ying Zhang[1,*]
Xiaowen Wu[1,*]
Chenxi Hou[1]
Kun Shang[1]
Kui Yang[1]
Zhimin Tian[2]
Zhichao Pei[1]
Yongquan Qu[2]
Yuxin Pei[1]

[1]Shaanxi Key Laboratory of Natural Products & Chemical Biology, College of Chemistry and Pharmacy, Northwest A&F University, Yangling, Shaanxi, People's Republic of China; [2]Center for Applied Chemical Research, Frontier Institute of Science and Technology, Xi'an Jiaotong University, Xi'an, People's Republic of China

*These authors contributed equally to this work

Objective: The aim was to produce the first report of assembling degradable stimuli-responsive dithio-polydopamine coating with a cancer target unit for synergistic and targeted drug delivery.

Methods: A multifunctional drug delivery system was constructed by coating a dual-responsive dithio-polydopamine (PDS) on porous CeO_2 nanorods and subsequent conjugation of lactose derivative, where the PDS was formed by self-polymerization of dithio-dopamine (DOPASS).

Results: The multifunctional drug delivery system displayed excellent cancer targeted ability resulting from the conjugation of lactose derivative, which could specifically recognize the overexpressed asialoglycoprotein receptors on the surface of HepG2 cells. It also showed a dual-responsive property of glutathione and pH, achieving controllable drug release from the cleavage of disulfide bond and subsequent degradation of PDS in cancer cells. Moreover, the degradation of PDS led to the exposure of CeO_2 nanorods, which has a synergistic anticancer effect due to its cytotoxicity to cancer cells.

Conclusion: This work presents a good example of a rational design towards synergistic and targeted DDS for cancer chemotherapies.

Keywords: degradable polydopamine, cerium oxide nanoparticles, dual-responsiveness, targeted drug delivery, synergistic anticancer

Introduction

Multi-functional drug delivery systems (MDDSs) with targeting and stimulus-sensitive attributes, as an active research area,[1–9] can target the site of cancer cells to enhance the intracellular delivery of a drug and respond to local stimuli that are characteristic of the pathological site by shedding a protective coating and releasing entrapped drug to minimize undesired side-effect in normal cells in chemotherapy.[10–12] Meanwhile, degradable polymer coatings have been widely used in drug delivery systems due to their excellent drug blocking capacity and biodegradability,[13] where degradable polymers are often combined with targeting units to achieve targeted MDDS with stimuli-responsive functions which are responsive to the microenvironment of cancer cells (temperature,[14,15] pH,[16–19] glutathione (GSH) concentration,[20–22] or light[23–25]). In addition, MDDS with enhanced cytotoxicity to cancer has been recognized as a new approach in developing a synergistic MDDS.[26–29] However, there are only a few reports on fabricating both responsive and targeted polymers for synergistic drug delivery.[30,31]

Polydopamine (PDA)-based substrate-independent coating, due to its adhesive property,[32] has been comprehensively applied in nanomedicine for drug delivery

Correspondence: Yuxin Pei
Shaanxi Key Laboratory of Natural Products & Chemical Biology, College of Chemistry and Pharmacy, Northwest A&F University, Yangling, 712100 Shaanxi, People's Republic of China
Tel +86 29 8709 1196
Email peiyx@nwafu.edu.cn

submit your manuscript | www.dovepress.com
Dovepress
http://dx.doi.org/10.2147/IJN.S152002

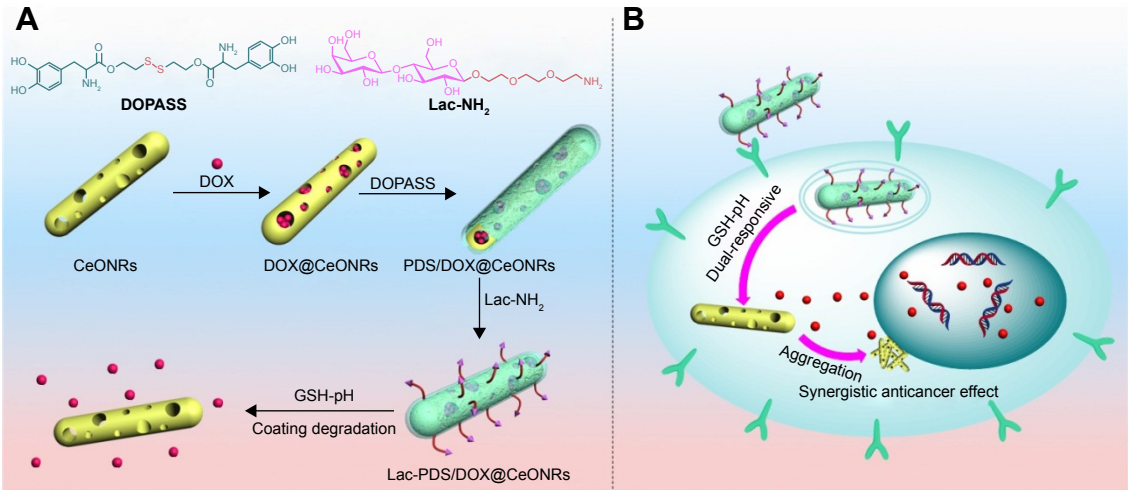

Scheme 1 Cartoon representation of (**A**) the construction process of the Lac-PDS/DOX@CeONRs and drug release upon the degradation of PDS under GSH and low pH; (**B**) its possible cellular pathway.
Abbreviations: PDS, dithio-polydopamine; DOX, doxorubicin hydrochloride; CeONR, CeO_2 nanorod; GSH, glutathione.

systems (DDS).[33–36] One valuable feature of PDA lies in its chemical structure that incorporates many functional groups such as catechol, amine, and imine, which further realize the emergence of diverse hybrid materials.[37–40] Frank's group immobilized pH-cleavable polymer-drug in PDA capsules via robust thiol-catechol reactions for intracellular drug delivery, which realized the application of pH stimuli-responsive PDA capsules as DDS.[41] However, the high adhesiveness and non-compatibility with degradability have made PDA limited in its application in MDDS.[42] Unfortunately, there are no reports on using degradable PDA for DDS, although Choi's group synthesized a degradable PDA film which was used for drug control release in GSH buffer solution.[42] Therefore, we envisioned that if degradable PDA could be combined with various functional materials, it may easily allow for the construction of a MDDS possessing both targeted and synergistic anticancer properties.

Cerium oxide nanoparticles (CeONPs) have been regarded as a promising biomaterial for biomedical applications[43–50] due to their excellent properties.[51] Previous studies have shown that CeONPs are cytotoxic to cancer cells, inducing oxidative stress and causing lipid peroxidation and cell membrane leakage.[52] It is also reported the CeO_2 could cause reactive oxygen species (ROS) damage to cancer cells.[53] As for drug delivery devices, CeONPs with pharmacological potential[54] could be used as nanocarriers and also act as therapeutic agents due to the DNA damage inflicted by CeONPs under acidic microenvironments.[55–57] For instance, by utilizing the synergistic anticancer effect of CeONPs, our group has constructed a synergistic and targeted DDS by immobilizing a galactose functioned pillar[5]arene on CeONRs via host-guest interaction.[27] Therefore, the distinct characters of CeONPs have enabled them to become an excellent candidate for synergistic drug delivery in cancer therapy.

Having been inspired by the distinctive and multi-faceted properties of PDA and CeONPs, we envisioned that, if PDA could be coated on the surface of CeONPs and could be easily degraded under a specific microenvironment in cancer cells, both the antitumor effect of drugs and the synergistic antitumor effect of CeONPs could be exerted. To the best of our knowledge, using degradable dual-responsive PDA as a coating on CeONPs for synergistic and targeted drug delivery has not been reported yet.

As shown in Scheme 1A, a dopamine derivative (DOPASS), was synthesized by linking two dopamine moieties through a disulfide bond. The self-polymerization of DOPASS yielded a polymer (PDS) which degrades in the presence of GSH. Thus, a new drug delivery vehicle was fabricated by coating PDS on the surface of porous CeONRs. To achieve the target ability of cancer cells, lactose was conjugated to the surface of the as-fabricated nanocarrier via Michael addition or Schiff base formation between PDS and lactose derivative (Lac-NH_2). With this kind of MDDS, the CeONRs could not only act as nanocarriers, but also could exhibit a synergistic anti-tumor effect on cancer cells as the PDS was degraded by high GSH concentration and low pH to expose the cytotoxic CeONRs in cancer cells.

Materials and methods

Materials

All reagents were purchased from commercial suppliers and used without further purification unless specified. Triple-distilled

water was used in this work. Doxorubicin hydrochloride (DOX) was purchased from Sangon Biotech (Shanghai, China). 3,4-dihydroxy-L-phenylalanine (L-DOPA), tert-butyldimethylsilyl chloride (TBDMSCl) and trifluoroacetic acid (TFA) were purchased from Tianjin xi'ensi Biochemical Technology Co., Ltd. (Tianjin, China). A dialysis bag was purchased from USA Viskase (Lombard, IL, USA) with a molecular weight cutoff of 8,000. N-[(tert-Butoxy)carbonyl]-L-tryptophan (Boc-Trp-OH), N,N-Diisopropylethylamine (DIPEA) and N,N,N′,N′-tetramethyl-O-(1H-benzotriazol-1-yl)uranium hexafluorophosphate (HBTU) were purchased from Energy Chemical Reagent Co (Shanghai, China). 2-[2-(2-chloroethoxy)ethoxy]ethanol was purchased from Jiu Ding Chemistry Reagent Co (Shanghai, China). 1,8-diazabicyclo[5.4.0]undec-7-ene (DBU) was purchased from Aladdin Reagent Co. (Shanghai, China). The human embryonic kidney T cells (293T) and hepatoma cells (HepG2) were obtained from KeyGEN BioTECH Co. (Nanjing, China).

Instrument

NMR spectra were recorded on a Bruker 500 MHz Spectrometer (Bruker Corporation, Karlsruhe, Germany), with working frequencies of 500 MHz for ^1H and 125 MHz for ^{13}C. The residual signals from DMSO-d_6 (^1H: δ2.50 ppm; ^{13}C: δ39.52 ppm) or $CDCl_3$ (^1H: δ7.26 ppm; ^{13}C: δ77.16 ppm) were used as internal standards. Negative-stained transmission electron microscope (TEM) images were taken on an HT7700 instrument (Hitachi Ltd., Tokyo, Japan, 80 kV). The samples for negative-stained TEM were prepared by dropping a droplet of the sample solution onto a TEM grid (copper grid, 300 mesh, coated with carbon film). The ζ potentials and dynamic light scattering (DLS) measurements of the nanoparticles at different fabrication stages were measured using a DelsaTM Nano system (Beckman Coulter, Brea, CA, USA). Cell culture was carried out in an incubator with a humidified atmosphere of 5% CO_2 at 37°C. UV-Vis spectra were recorded with a Shimadzu 1750 UV-visible spectrophotometer (Kyoto, Japan) at 298 K. The DOX absorbance and the MTT data were obtained from a microplate reader (Tecan Infinite M1000 Pro, Männedorf Switzerland), with a λ range from 230 nm to 1,000 nm. The surface area was measured by nitrogen physisorption (Quantachrome, Autosorb-iQ) based on the Brunauer–Emmet–Teller (BET) method (ASAP 2020, Micromeritics Inc, GA, USA).

Method

Preparation of PDS/DOX@CeONRs

The CeONRs were made by following the procedure reported previously.[58] Briefly, $Ce(NO_3)_3{\cdot}6H_2O$ (1.736 g) and NaOH (19.2 g) were dissolved in 10 and 70 mL of millipore water (MQ water, 18.2 MΩ cm), respectively. The two solutions were thoroughly mixed in a Pyrex bottle, and the mixture was treated with continuous stirring for 30 min. Subsequently, the Pyrex bottle was transferred into a temperature-controlled electric oven at 100°C for 24 h. After natural cooling to room temperature, the solid products were collected by centrifugation, and washed with MQ water and ethanol three times, and dried at 60°C overnight. Then, the non-porous nanorod precursor (20 mg) was dispersed in 10 mL of MQ water by sonication. The porous nanorods of ceria were obtained under hydrothermal conditions in an autoclave at 160°C for 12 h. The pale-yellow solid product was collected by centrifugation, washed with MQ water and ethanol, and dried at 60°C overnight.[58] DOPASS was prepared by adapting previously reported procedure[42] (see Scheme S1 in the supporting information and Figures S1–S4 are the NMR data for respective compounds). For DOX loading, CeONRs (50 mg) were added to water solution of DOX (6 mL, 1 mg/mL) and stirred for 24 h. The solution was centrifuged and washed with water to move the remaining DOX from the surface of CeONRs. DOX-loaded CeONRs (DOX@CeONRs) were dried at 40°C under vacuum. DOX@CeONRs (50 mg) were dispersed in 20 mL of Tris–HCl buffer (pH 8.5, 10 mM), and then 26 mg DOPASS was added. The mixture was stirred for 4 h in the dark at room temperature. PDS-coated DOX@CeONRs (PDS/DOX@CeONRs) were then centrifuged and washed several times with deionized water to remove the unpolymerized DOPASS.

Preparation of Lac-PDS/DOX@CeONRs

NH_2-Lactose was prepared by adapting a previously reported procedure,[59] (see Scheme S2 in the supporting information, Figures S5 and S6 are the NMR data for respective compounds). The freeze-dried PDS/DOX@CeONRs (15 mg) were added to phosphate-buffered saline (PBS) (pH=7.4, 10.0 mL) solution of NH_2-Lactose (20 mg, 0.04 mmol) and stirred for 1 h. In the end, Lac-PDS/DOX@CeONRs were obtained by centrifugation and washed with deionized water three times to remove the surplus Lac-NH_2.

Drug loading content of Lac-PDS/DOX@CeONRs

During the preparation of Lac-PDS/DOX@CeONRs, all the washings and supernatants after loading were collected and combined as presented in the previous report.[33] The remaining DOX was analyzed by a microplate reader at absorbance of 490 nm. The content of the remaining DOX was calculated according to a calibration curve. The loading content of

Lac-PDS/DOX@CeONRs was calculated by the following equation:[31]

$$LC = \frac{\text{Weight of initial DOX} - \text{Weight of remaining DOX}}{\text{Weight of the nanoparticles}}$$

Drug release experiments in vitro

Freeze-dried Lac-PDS/DOX@CeONRs (20 mg) and DOX@CeONRs (20 mg) were dispersed in 1 mL of PBS (containing NaCl 137 mmol/L, KCl 2.7 mmol/L, Na_2HPO_4 10 mmol/L, KH_2PO_4 2 mmol/L, and adjusting to pH=7.4) and transferred into dialysis bags (molecular weight cutoff=8,000, respectively). Then the bags were submerged at 15 mL solution with different pH values (7.4 and 5.0) or GSH values (2.5 mM and 10.0 mM, respectively) and stirred at 37°C. At designated time intervals, the solution out of the bags was transferred into a test tube for microplate reader.

Cell culture

293T cells were cultured in a medium containing 10% FBS (fetal bovine serum) and 1% penicillin/streptomycin (complete DMEM; Dulbecco's Modified Eagle's Medium [Thermo Fisher Scientific, Waltham, MA, USA]) in 5% CO_2 at 37°C. HepG2 cells were cultured in RPMI 1640 medium containing 10% FBS and 1% penicillin/streptomycin (complete 1640) in 5% CO_2 at 37°C.

Targeting ability of Lac-PDS/CeONRs using flow cytometer and CLSM

HepG2 cells were seeded in 6-well plates (1×10^5 cells/well) and cultured in RPMI 1640 medium for 24 h. The fresh medium containing 5 μM free DOX, Lac-PDS/DOX@CeONRs or PDS/DOX@CeONRs were added, respectively. In contrast, one group was pretreated with lactobionic acid (LA, 2 mg/mL) for 4 h before the incubation with Lac-PDS/DOX@CeONRs. After 4 h, the cells were collected and washed two times with cold PBS and resuspended in 500 μL PBS. Finally, the cell were analyzed by a flow cytometer (Beckman Coulter Cytomics Altra).

HepG2 cells were seeded in 35 mm plastic bottomed μ-dishes for 24 h, and then the medium was replaced with a fresh one. The cells were treated with Lac-PDS/DOX@CeONRs for 4 h. In contrast, one group was pre-incubated with LA (2 mg/mL) for 4 h to block the lactose receptor on the surface of HepG2 cells before the incubation with Lac-PDS/DOX@CeONRs. After 4 h, the cells were collected and washed two times with cold PBS. Then the cells were fixed by the 4% formaldehyde for 15 min and stained with DAPI (4′,6-diamidino-2-phenylindole) for 10 min. Meanwhile, the target ability of Lac-PDS/DOX@CeONRs which resulted from the lactose derivative was confirmed by confocal laser scanning microscopy (CLSM).

Cytotoxicity assay

The in vitro cytotoxicity was measured by MTT assay.[60–62] The relative cell viability of different corresponding compounds (CeONRs, Lac-PDS/CeONRs, DOX, or Lac-PDS/DOX@CeONRs) was evaluated in vitro by MTT assay. The cells were seeded in 96-well plates at a density of 5×10^3 cells per well in 100 μL complete DMEM or 1640 and grew for 24 h at 37°C. Subsequently, the cells were incubated with the corresponding compounds at different concentrations for 24 h, 48 h, and 72 h, respectively. The cells were washed and the fresh medium containing MTT was added into each plate. The cells were incubated for another 4 h. After removing the medium containing MTT, dimethyl sulfoxide (100 μL) was added to each well to dissolve the formazan crystals. Finally, the plate was gently shaken for 10 min, and the absorbance at 490 nm was recorded with a microplate reader.

Western blot analysis

Total protein from cultured cells was harvested in an extraction buffer (Beyotime, Shanghai, China) supplemented with protease and phosphatase inhibitors (Pierce, Rockford, IL, USA). Briefly, protein samples were separated using 10% SDS-PAGE gels, then transferred to polyvinylidene difluoride membranes (Millipore, Bedford, MA, USA). The membranes were blocked with 5% nonfat dry milk in TBS containing 0.1% Tween for 1 h at room temperature and then blotted with primary antibodies: anti-Casp9 (1:100), anti-Actin (1:1,000) overnight. After washing, the membranes were incubated with a secondary horseradish peroxidase (HRP)-coupled antibody and visualized using Immobilon HRP substrate (Millipore, Billerica, MA, USA). The density of the bands was quantified using ImageJ Software (National Institute of Health, Bethesda, MD, USA). The ratio of the intensity of the target protein to that of β-tubulin loading control was calculated to represent the expression level of the protein.

Results and discussion

Characterization and functionalization of Lac-PDS/CeONRs

The CeONRs were made in our group, which had an average length and diameter of about 60 nm and 5.8±1 nm, respectively. The PDS coated CeONRs (PDS@CeONRs) were investigated by FT-IR spectroscopy (Figure S7), which showed an

absorption band at 2,900–3,000 cm^{-1}, corresponding to the *v* (C–H), 1,200–1,300 cm^{-1}, corresponding to the *v* (C–O), and 1,600–1,700 cm^{-1}, corresponding to the *v* (C=O),[42,63] confirming the successful coating of PDS on the surface of CeONRs. In addition, the ζ potential changed from 1.84±0.35 mV for CeONRs to −8.29±0.43 mV after coating PDS on CeONRs. Lactose was conjugated to the surface of PDS@CeONRs (Lac-PDS@CeONRs) via Michael addition reaction, which leads to a lower ζ potential of −14.65±0.17 mV (Table S1).

The stability of Lac-PDS@CeONRs in aqueous solution was investigated. By dispersing the Lac-PDS@CeONRs in PBS buffer and cellular 1640 culture medium via sonication for 15 min, no precipitate was observed after the suspensions were left standing for at least 1 day (Figure S8D). Furthermore, the characterization by TEM revealed the CeONRs had an average length and diameter of 60 nm and 6 nm, respectively (Figure 1A). According to a recent study,[64] rod-like nanoparticles exhibited higher cellular internalization than sphere-like nanoparticles. A 3 nm layer was also detected after coating PDS on CeONRs (Figure 1B), which further confirmed the successful coating of PDS on the surface of CeONRs. Moreover, Lac-PDS@CeONRs had a thicker layer compared to the PDS@CeONRs, resulting from the conjugation of lactose derivative (Figure 1C), and the DLS data also complied with the results (Figure S8A–C).

Upon addition of glutathione (10 mM), the distinct layer in TEM observed previously disappeared (Figure 1D), due to the degradation of PDS via reduction of disulfide bond in the PDS film.[42] This result confirmed the stimuli-responsive property of PDS, and consolidated its potential candidacy for application in DDS. Furthermore, a similar phenomenon was also observed from immersing a PDS coated silicon slice (Figure S9A and C) in 10 mM GSH using a scanning electron microscope (SEM), where the coated surface was destroyed by the high concentration of GSH (Figure S9B and D).

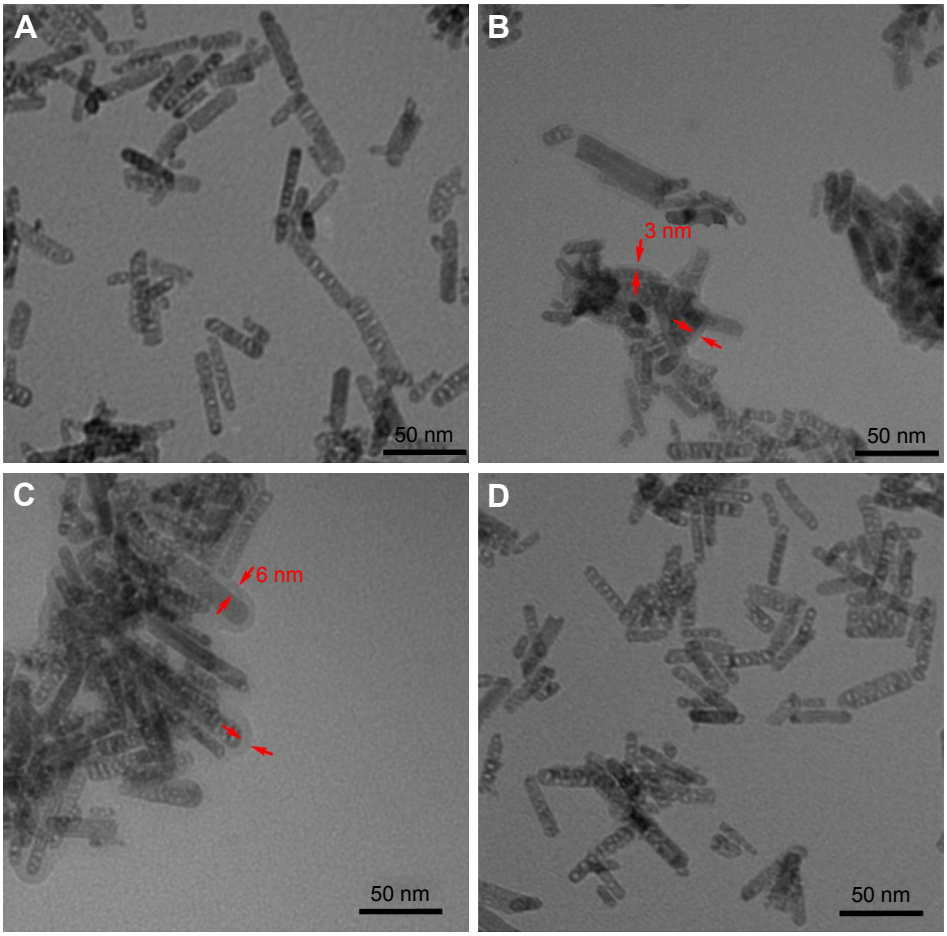

Figure 1 TEM images of (**A**) CeONRs; (**B**) PDS@CeONRs; (**C**) Lac-PDS@CeONRs; and (**D**) Lac-PDS@CeONRs after being treated with 10 mM GSH for 6 h.
Note: The thickness of the PDS layer coated on the CeONRs were indicated by red arrows.
Abbreviations: TEM, transmission electron microscope; CeONR, CeO_2 nanorod; PDS, dithio-polydopamine; GSH, glutathione.

Study of drug loading and releasing profile

Next, a study of drug loading and releasing profiles of CeONRs was conducted by using DOX as a model drug. First, the drug-loading capacity of CeONRs was investigated by mixing CeONRs with different concentrations of DOX. As illustrate in Figure S10, the amount of DOX loaded in CeONRs increased with the increasing of initial DOX concentration, and the drug-loading capacity achieved a highest level of 11.4%, which confirmed that the CeONRs can be used as the platform for drug delivery. The porosity and surface area of CeONRs were tested by nitrogen physisorption based on the BET method, where the pore size distribution and the N_2 adsorption-desorption isotherms (Figure S11 and Table S2, and the average pore size and pore volume is 11.98 nm and 0.36 cm^3/g, respectively) further confirmed the porosity of CeONRs for drug loading. Subsequently, after coating PDS on the drug loaded CeONRs and conjugating lactose on its surface, the system was dispersed in different mediums after sonication. As shown in Figure S12, the DOX loaded uncoated CeONRs (DOX@CeONRs) were placed in PBS, where a rapid release was observed. However, the presence of PDS coating kept the DOX loaded nano carrier in a closed configuration. Accordingly, there was no significant DOX leakage (<10%) in neutral PBS solution (Figure 2). However, upon decreasing the pH of PBS to 5.0, a higher level of release was observed (50%). Moreover, when the Lac-PDS/DOX@CeONRs were treated with different concentrations of GSH, an even higher level of release was observed with the increase of GSH concentration with pH 5.0 (55% in 2.5 mM GSH; 80% in 10 mM GSH). These results indicated that the PDS had an excellent drug blocking function for nano carriers, which was stable under normal physiological conditions. Meanwhile, the mimetic cancer cell microenvironment (low pH and high GSH concentration) demonstrated the sensitive stimuli-responsiveness to cancer cell microenvironment which was essential for controllable drug release.

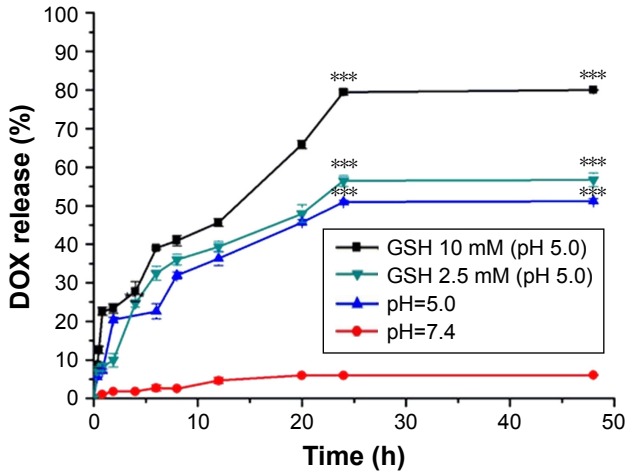

Figure 2 DOX release profiles from Lac-PDS/DOX@CeONRs in PBS at different GSH concentrations and different pH values.
Note: ***$P<0.001$.
Abbreviations: DOX, doxorubicin hydrochloride; PDS, dithio-polydopamine; CeONR, CeO_2 nanorod; PBS, phosphate-buffered saline; GSH, glutathione.

Study of stimuli-responsiveness of Lac-PDS/DOX@CeONRs

The GSH-responsive property and cellular uptake efficiency of Lac-PDS/DOX@CeONRs were further studied by CLSM using live HepG2 (a hepatoma carcinoma cell) cells. The results were shown in Figure 3 (Figure 3M–P for the free DOX group). As shown in Figure 3I–L, red fluorescence of DOX in the HepG2 cells was observed clearly after incubation with Lac-PDS/DOX@CeONRs (DOX concentration 5.0 μM) for 4 h. In contrast, an obvious fluorescence enhancement was shown with the addition of GSH (10.0 mM) to the culture medium (Figure 3A–D), which was attributed to the accelerated DOX release progress due to the cleavage of the disulfide bond to degrade PDS in a higher intracellular GSH concentration.

Study of targeted ability of Lac-PDS/DOX@CeONRs

Meanwhile, the target ability of Lac-PDS@CeONRs resulting from the lactose derivative was confirmed by CLSM, where the HepG2 cells were cultivated with Lac-PDS/DOX@CeONRs for 4 h. To compare, one group was pre-incubated with LA for 4 h to block the lactose receptors on the surface of HepG2 cells, which showed a dramatic decrease in fluorescence of DOX (Figure 3E–H). Furthermore, its target ability was further confirmed by flow cytometry (Figure 4). The HepG2 cells were incubated with DOX, PDS/DOX@CeONRs, and Lac-PDS/DOX@CeONRs, respectively, at 5 μM for 4 h. To compare, one group was pretreated with LA as a targeting inhibitor before incubation with Lac-PDS/DOX@CeONRs. As shown in Figure 4F, the Lac-PDS/DOX@CeONRs group (orange line) had the strongest fluorescence intensity compared with the free DOX group (blue line) and the PDS/DOX@CeONRs group (green line), which lacks the lactose target unit. The Lac-PDS/DOX@CeONRs group that was pre-incubated with LA (dark green line) displayed the weakest fluorescence intensity due to the blockade of the asialoglycoprotein receptors by LA, which subsequently led to the inhibition of lactose residue mediated endocytosis.

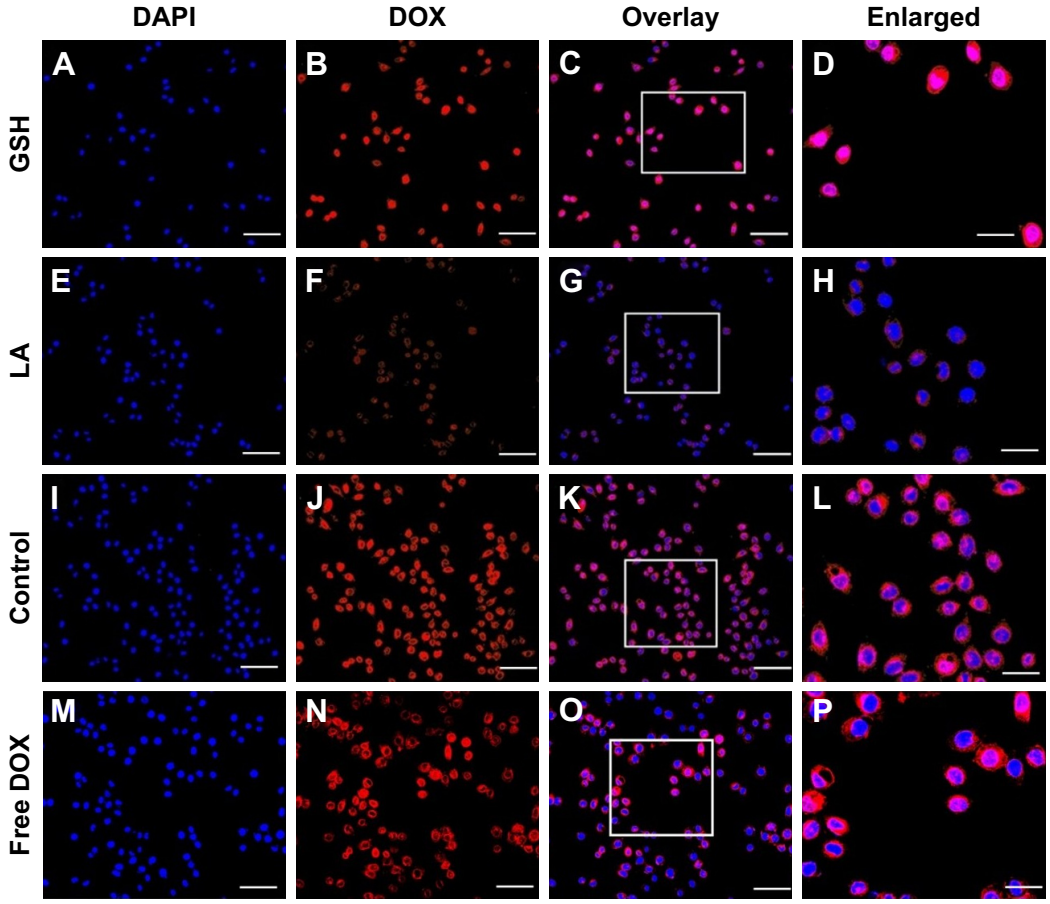

Figure 3 CLSM images of HepG2 cultured with Lac-PDS/DOX@CeONRs in the presence of 10 mM GSH for 4 h (**A**–**D**); HepG2 cultured with Lac-PDS/DOX@CeONRs for 4 h preincubated with LA for 4 h (**E**–**H**); HepG2 cultured with Lac-PDS/DOX@CeONRs as control (**I**–**L**) for 4 h; HepG2 cultured with free DOX (**M**–**P**). The DOX concentration is 5.0 μM. The nuclei were stained with DAPI; images were taken from DAPI channel (**A**, **E**, **I**, **M**), DOX channel (**B**, **F**, **J**, **N**), and the overlapped images (**C**, **G**, **K**, **O**). Scale bar: 50 μm (**A**–**C**, **E**–**G**, **I**–**K**, and **M**–**O**); the enlarged view of the marked area (**D**, **H**, **L**, **P**). Scale bar: 20 μm (**D**, **H**, **L**, and **P**).
Abbreviations: CLSM, confocal laser scanning microscopy; PDS, dithio-polydopamine; DOX, doxorubicin hydrochloride; CeONR, CeO_2 nanorod; GSH, glutathione; LA, lactobionic acid; DAPI, 4′,6-diamidino-2-phenylindole.

Study of cytotoxicity of materials

To study the cytotoxicity of the materials for DDS, 293T cells (normal cells) and HepG2 cells were incubated with CeONRs and Lac-PDS@CeONRs, respectively, at different concentrations. As shown in Figure 5A, the CeONRs showed low cytotoxicity to 293T cells and HepG2 cells. However, after coating with PDS and conjugating the lactose, the Lac-PDS@CeONRs showed low toxicity to 293T cells but enhanced high toxicity to HepG2 cells (Figure 5B). We deduced that these results were due to more aggregation resulting from the lactose mediated endocytosis and the acid environment and high GSH concentration of cancer cells which triggered cytotoxicity to cancer cells from the degradation of PDS, and exposure of the CeONRs to an acid environment in cancer cells. Therefore, these results indicated not only the excellent biocompatibility of Lac-PDS@CeONRs for 293T cells, which is essential for design of DDS, but also the enhanced cytotoxicity to cancer cells resulting from CeONRs, which could be applied in synergistic drug delivery.

Moreover, the synergistic antitumor effect of the DDS was further confirmed by incubating HepG2 and 293T cells, respectively, with Lac-PDS/DOX@CeONRs in comparison to free DOX. As shown in Figure 5C, the Lac-PDS/DOX@CeONRs showed low toxicity to 293T cells compared to free DOX and showed relative excellent toxicity to HepG2 cells (Figure 5D). Moreover, the cell viability of HepG2 cells incubated with Lac-PDS/DOX@CeONRs and free DOX at different concentrations for 24 h, 48 h, and 72 h was conducted, respectively (Figure S13). The cell viability of HepG2 cells incubated with Lac-PDS/DOX@CeONRs and DOX@CeONRs at 24 h and 48 h was also conducted (Figure S14), respectively. When the Lac-PDS/DOX@CeONRs were delivered into cancer cells, the high concentration of GSH

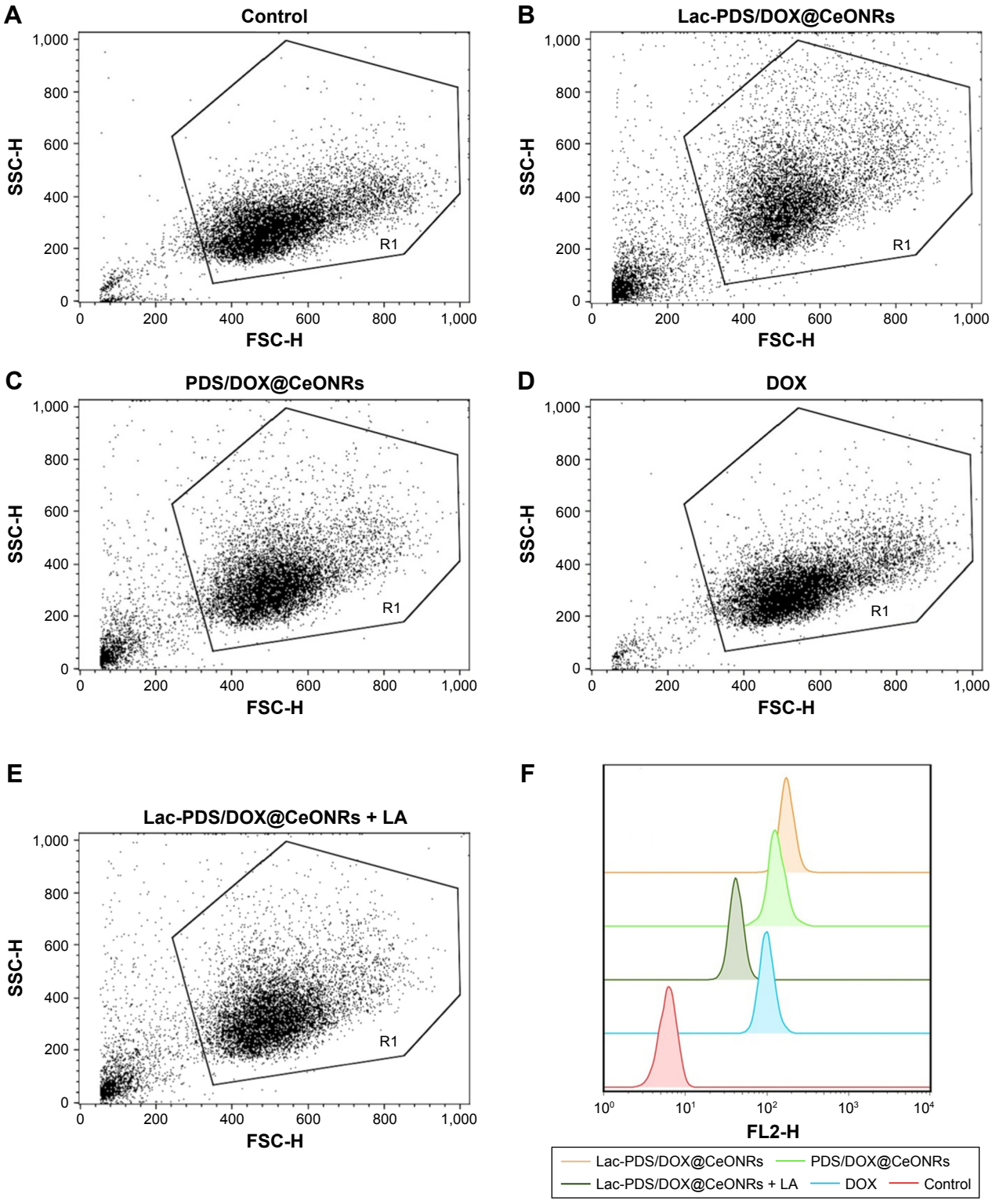

Figure 4 Flow cytometry analysis of HepG2 cells after incubation for 4 h with Lac-PDS/DOX@CeONRs (**B**: orange line in **F**); PDS/DOX@CeONRs (**C**: green line in **F**); 5 μM DOX (**D**: blue line in **F**); Lac-PDS/DOX@CeONRs after pre-incubation with LA for 4 h (**E**: dark green line in **F**) and control (**A**: red line in **F**).
Abbreviations: PDS, dithio-polydopamine; DOX, doxorubicin hydrochloride; CeONR, CeO_2 nanorod; LA, lactobionic acid.

and low pH in cancer cells could enable the cleavage of disulfide linkage and, consequently, degraded PDS coating to release the drugs and expose the surface of CeO_2. Thus, the synergistic effect was produced by CeONRs exposure and DOX releasing in cancer cells, where CeONRs not only act as the drug container, but also as the anti-cancer agent itself. Subsequently, it was further confirmed that the increased toxicity was caused by the high concentration of GSH in

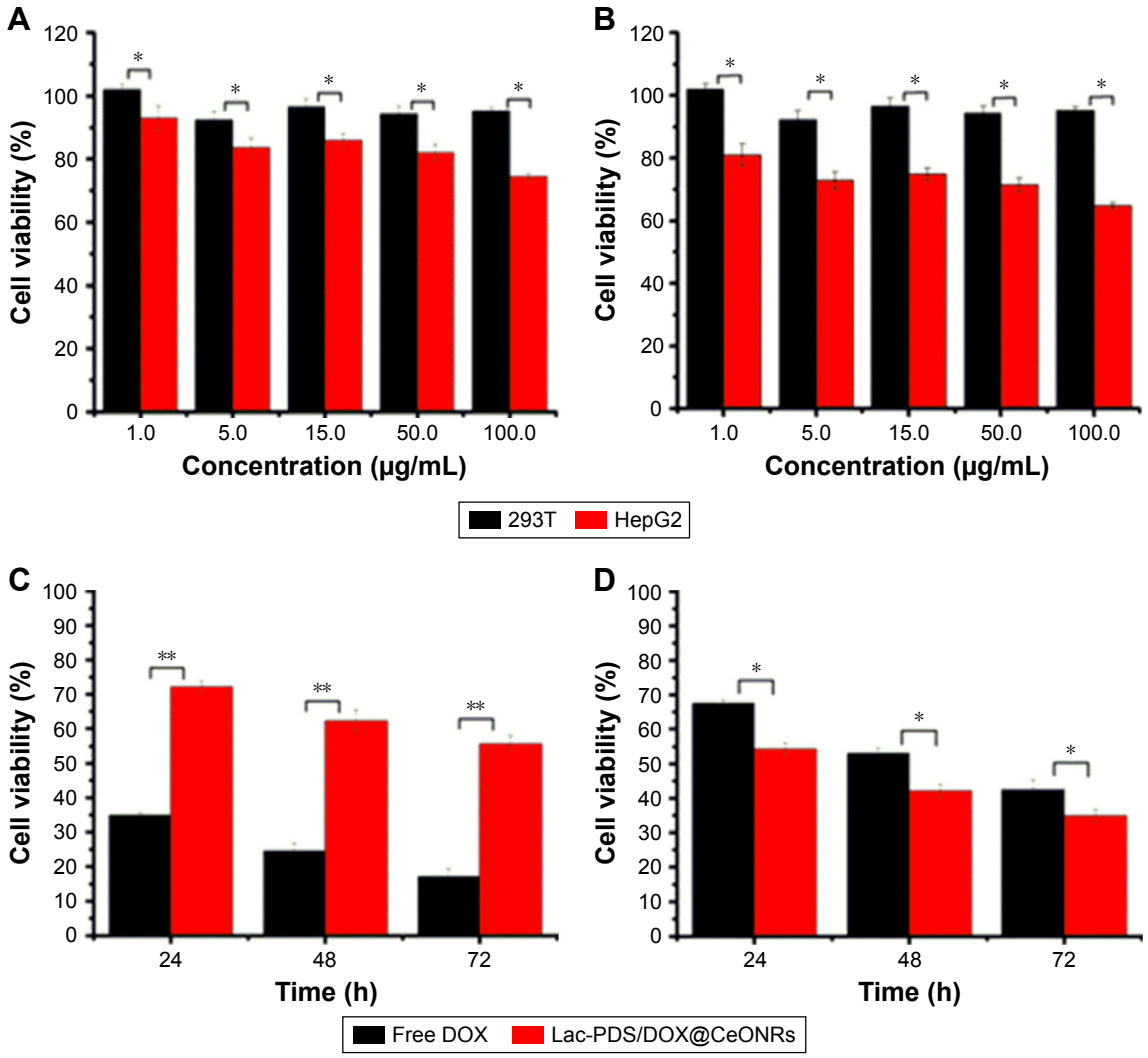

Figure 5 (**A**) Cell viability of HepG2 cells and 293T cells incubated with CeONRs for 24 h; (**B**) Cell viability of HepG2 cells and 293T cells incubated with Lac-PDS/CeONRs for 24 h; (**C**) Cell viability of 293T cells incubated with Free DOX and Lac-PDS/DOX@CeONRs for 24 h, 48 h, and 72 h; (**D**) Cell viability of HepG2 cells incubated with Free DOX and Lac-PDS/DOX@CeONRs for 24 h, 48 h, 72 h. The DOX concentration is 1 μg/mL (*$P<0.5$; **$P<0.01$).
Abbreviations: CeONR, CeO_2 nanorod; PDS, dithio-polydopamine; DOX, doxorubicin hydrochloride.

cancer cells which degraded the PDS from CeONRs and exposed the surface of CeO_2, which synergistically enhanced the toxicity of DOX to the tumorous HepG2 cells.

Study of the location of Lac-PDS/DOX@CeONRs in HepG2 cells

Further study of HepG2 cells incubated with Lac-PDS/DOX@CeONRs and CeONRs by TEM disclosed that the nano rods were aggregated in the nuclear peri-region of the HepG2 cells incubated with Lac-PDS/DOX@CeONRs (Figure 6C) and CeONRs (Figure S15), in contrast with the blank control (Figure 6A and B), the rod shape nanoparticles in the enlarged panel (Figure 6D) were observed, which was in agreement with the reported literature.[51]

However, according to the CLSM image in Figure 7, when HepG2 cells were stained with Hoechst 33258 after being cultured with CeONRs for 24 h, a distinguished chromatin condensation was found. Apart from that, in Figure 8, a Western blot analysis for Casp9 was conducted. Also, a relatively higher concentration of Casp9 was observed after cultured HepG2 cells with CeONRs or Lac-PDS/CeONRs for 24 h compared with the control group. Thus, these aggregated CeO_2 particles in the perinuclear region may activate caspase and further cause chromatin condensation, which may finally lead to HepG2 cells apoptosis, which is in accordance with the reported research.[51] The results indicated that CeONRs act not only as the drug container, but also as the synergetic antitumor agent.

Conclusion

A synergistic and targeted drug delivery system Lac-PDS/DOX@CeONRs based on porous CeONRs coated with degradable PDS and conjugated with lactose derivative was

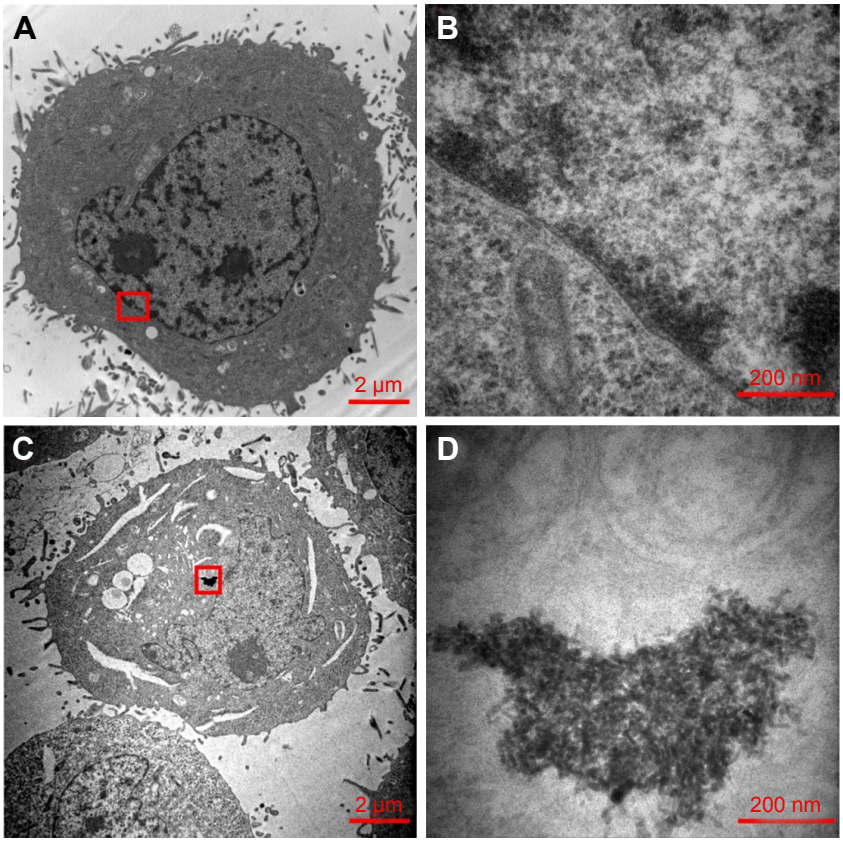

Figure 6 (**A**) TEM image of HepG2 in blank control. (**B**) Enlarged view of the marked area of panel **A**. (**C**) TEM image of HepG2 incubated with Lac-PDS/DOX@CeONR at 5 μM for 24 h. (**D**) Enlarged view of the marked area of panel **C**.
Abbreviations: TEM, transmission electron microscope; PDS, dithio-polydopamine; DOX, doxorubicin hydrochloride; CeONR, CeO_2 nanorod.

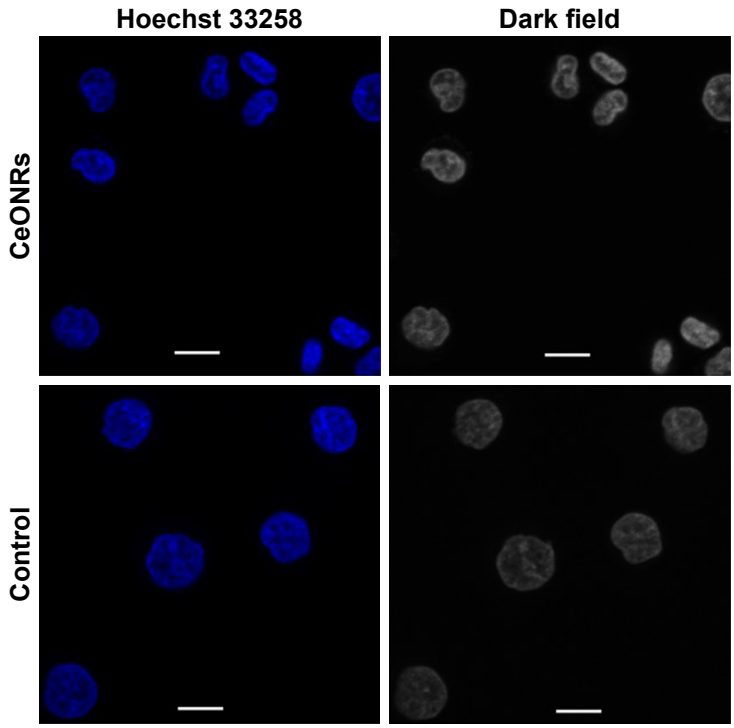

Figure 7 CLSM images of HepG2 cultured with 40 μg/mL CeONRs, and the control group cultured with the same amount of PBS. Scale bar: 5 μm.
Abbreviations: CLSM, confocal laser scanning microscopy; CeONR, CeO_2 nanorod; PBS, phosphate-buffered saline.

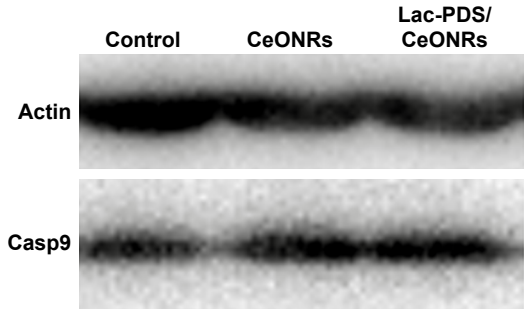

Figure 8 Western blot analysis for Casp9, HepG2 cells cultured with 40 μg/mL CeONRs and Lac-PDS/CeONRs, and the control group treated with the same amount of PBS.
Abbreviations: CeONR, CeO_2 nanorod; PDS, dithio-polydopamine; PBS, phosphate-buffered saline.

developed, which exhibited GSH and pH responsiveness and cancer target ability resulting from the disulfide bond of PDS and the conjugated lactose, respectively. Lac-PDS/DOX@CeONRs not only exhibited excellent GSH and pH responsiveness and quick release of DOX upon the degradation of PDS from CeONRs resulting from low pH and high GSH concentration in cancer cells, but also showed hepatoma-targeting ability to ASGP-R overexpressing HepG2 cells. As expected, the Lac-PDS@CeONRs not only displayed biocompatible properties in normal cells, but also showed a synergistic anti-cancer effect resulting from the degradation of PDS coating and exposure of CeONRs in cancer cells. Also, the TEM, CLSM, and Western blot analysis demonstrated the chromatin condensation resulting from CeONRs, which confirmed the anticancer effect of CeONRs. Thus, this work provides a novel strategy for rationale design in constructing unique nanocarriers towards synergistically enhanced cytotoxicity for cancer chemotherapies.

Acknowledgments

This research work was supported by the National Natural Science Foundation of China (NSFC 21772157 and 21572181), the Project of Science and Technology of Social Development in Shaanxi Province (2016SF-029). The authors thank Mr Yihan Pei for language help.

Disclosure

The authors report no conflicts of interest in this work.

References

1. Chang Y, Yang K, Wei P, et al. Cationic vesicles based on amphiphilic pillar[5]arene capped with ferrocenium: a redox-responsive system for drug/siRNA co-delivery. *Angew Chem Int Ed Engl*. 2014;53(48):13126–13130.
2. Hu X-Y, Liu X, Zhang W, et al. Controllable construction of biocompatible supramolecular micelles and vesicles by water-soluble phosphate pillar[5,6]arenes for selective anti-cancer drug delivery. *Chem Mater*. 2016;28(11):3778–3788.
3. Wu X, Tan YJ, Toh HT, et al. Stimuli-responsive multifunctional glyconanoparticle platforms for targeted drug delivery and cancer cell imaging. *Chem Sci*. 2017;8(5):3980–3988.
4. Chi X, Ji X, Shao L, Huang F. A multiresponsive amphiphilic supramolecular diblock copolymer based on pillar[10]arene/paraquat complexation for rate-tunable controlled release. *Macromol Rapid Commun*. 2017;38(4):1600626.
5. Yu G, Yu W, Shao L, et al. Fabrication of a targeted drug delivery system from a pillar[5]arene-based supramolecular diblock copolymeric amphiphile for effective cancer therapy. *Adv Funct Mater*. 2016;26(48):8999–9008.
6. Taghizadeh B, Taranejoo S, Monemian SA, et al. Classification of stimuli-responsive polymers as anticancer drug delivery systems. *Drug Deliv*. 2015;22(2):145–155.
7. Jahangirian H, Lemraski EG, Webster TJ, Rafiee-Moghaddam R, Abdollahi Y. A review of drug delivery systems based on nanotechnology and green chemistry: green nanomedicine. *Int J Nanomed*. 2017;12:2957–2978.
8. Zhang J, Wang Y, Chen J, et al. Inhibition of cell proliferation through an ATP-responsive co-delivery system of doxorubicin and Bcl-2 siRNA. *Int J Nanomed*. 2017;12:4721–4732.
9. Chang Y, Hou C, Ren J, et al. Multifunctional supramolecular vesicles based on the complex of ferrocenecarboxylic acid capped pillar[5]arene and a galactose derivative for targeted drug delivery. *Chem Commun*. 2016;52:9578–9581.
10. Torchilin VP. Multifunctional, stimuli-sensitive nanoparticulate systems for drug delivery. *Nat Rev Drug Discov*. 2014;13(11):813–827.
11. Mei L, Zhu G, Qiu L, et al. Self-assembled multifunctional DNA nanoflowers for the circumvention of multidrug resistance in targeted anticancer drug delivery. *Nano Res*. 2015;8(11):3447–3460.
12. Chang Y, Lv Y, Wei P, et al. Multifunctional glyco nanofibers: siRNA induced supermolecular assembly for codelivery in vivo. *Adv Funct Mater*. 2017;27(44).
13. Binauld S, Stenzel MH. Acid-degradable polymers for drug delivery: a decade of innovation. *Chem Commun*. 2013;49(21):2082–2102.
14. Wang SY, Liu MC, Kang KA. Magnetic nanoparticles and thermally responsive polymer for targeted hyperthermia and sustained anti-cancer drug delivery. *Adv Exp Med Biol*. 2013;765:315–321.
15. Zardad A-Z, Choonara YE, du Toit LC, et al. A review of thermo- and ultrasound-responsive polymeric systems for delivery of chemotherapeutic agents. *Polymers*. 2016;8(10):359.
16. Duan Z, Zhang Y, Zhu H, et al. Stimuli-sensitive biodegradable and amphiphilic block copolymer-gemcitabine conjugates self-assemble into a nanoscale vehicle for cancer therapy. *ACS Appl Mater Interfaces*. 2017;9(4):3474–3486.
17. Xu J, Luan S, Qin B, et al. Backbone-hydrazone-containing biodegradable copolymeric micelles for anticancer drug delivery. *J Nanoparticle Res*. 2016;18(11):316.
18. Huang X, Liao W, Zhang G, Kang S, Zhang CY. pH-sensitive micelles self-assembled from polymer brush (PAE-g-cholesterol)-b-PEG-b-(PAE-g-cholesterol) for anticancer drug delivery and controlled release. *Int J Nanomed*. 2017;12:2215–2226.
19. Zhu WJ, Yang SD, Qu CX, et al. Low-density lipoprotein-coupled micelles with reduction and pH dual sensitivity for intelligent co-delivery of paclitaxel and siRNA to breast tumor. *Int J Nanomed*. 2017;12:3375–3393.
20. Cai T, Chen Y, Wang Y, et al. One-step preparation of reduction-responsive biodegradable polymers as efficient intracellular drug delivery platforms. *Macromol Chem Phys*. 2014;215(19):1848–1854.
21. Zhou T, Zhao X, Liu L, Liu P. Preparation of biodegradable PEGylated pH/reduction dual-stimuli responsive nanohydrogels for controlled release of an anti-cancer drug. *Nanoscale*. 2015;7(28):12051–12060.
22. Xu Z, Liu S, Kang Y, Wang M. Glutathione-responsive polymeric micelles formed by a biodegradable amphiphilic triblock copolymer for anticancer drug delivery and controlled release. *ACS Biomater Sci Eng*. 2015;1(7):585–592.

23. You C, Wu H, Wang M, et al. Near-infrared light and pH dual-responsive targeted drug carrier based on core-crosslinked polyaniline nanoparticles for intracellular delivery of cisplatin. *Chemistry*. 2017; 23(22):5352–5360.
24. Ji Y, Zhao J, Chu CC. Biodegradable nanocomplex from hyaluronic acid and arginine based poly(ester amide)s as the delivery vehicles for improved photodynamic therapy of multidrug resistant tumor cells: an in vitro study of the performance of chlorin e6 photosensitizer. *J Biomed Mater Res A*. 2017;105(5):1487–1499.
25. Xia Y, Zeng Y, Hu D, et al. Light and pH dual-sensitive biodegradable polymeric nanoparticles for controlled release of cargos. *J Polymer Sci A Polym Chem*. 2017;55(10):1773–1783.
26. Yang K, Chang Y, Wen J, et al. Supramolecular vesicles based on complex of trp-modified pillar[5]arene and galactose derivative for synergistic and targeted drug delivery. *Chem Mater*. 2016;28(7):1990–1993.
27. Wu X, Zhang Y, Lu Y, et al. Synergistic and targeted drug delivery based on nano-CeO2 capped with galactose functionalized pillar[5]arene via host–guest interactions. *J Mater Chem B*. 2017;5(19):3483–3487.
28. Wu S, Yang X, Lu Y, et al. A green approach to dual-drug nanoformulations with targeting and synergistic effects for cancer therapy. *Drug Deliv*. 2017;24(1):51–60.
29. Dong DW, Xiang B, Gao W, Yang ZZ, Li JQ, Qi XR. pH-responsive complexes using prefunctionalized polymers for synchronous delivery of doxorubicin and siRNA to cancer cells. *Biomaterials*. 2013;34(20): 4849–4859.
30. Lee SJ, Yook S, Yhee JY, et al. Co-delivery of VEGF and Bcl-2 dual-targeted siRNA polymer using a single nanoparticle for synergistic anti-cancer effects in vivo. *J Control Release*. 2015;220(Pt B):631–641.
31. Zhu C, Xiao J, Tang M, Feng H, Chen W, Du M. Platinum covalent shell cross-linked micelles designed to deliver doxorubicin for synergistic combination cancer therapy. *Int J Nanomed*. 2017;12:3697–3710.
32. Ji M, Jiang N, Chang J, Sun J. Near-infrared light-driven, highly efficient bilayer actuators based on polydopamine-modified reduced graphene oxide. *Adv Funct Mater*. 2014;24(34):5412–5419.
33. Chang D, Gao Y, Wang L, et al. Polydopamine-based surface modification of mesoporous silica nanoparticles as pH-sensitive drug delivery vehicles for cancer therapy. *J Colloid Interface Sci*. 2016;463: 279–287.
34. Ge R, Li X, Lin M, et al. Fe_3O_4@polydopamine composite theranostic superparticles employing preassembled Fe_3O_4 nanoparticles as the core. *ACS Appl Mater Interfaces*. 2016;8(35):22942–22952.
35. Li Y, Jiang C, Zhang D, et al. Targeted polydopamine nanoparticles enable photoacoustic imaging guided chemo-photothermal synergistic therapy of tumor. *Acta Biomater*. 2017;47:124–134.
36. Li Z, Hu Y, Howard KA, et al. Multifunctional bismuth selenide nanocomposites for antitumor thermo-chemotherapy and imaging. *ACS Nano*. 2016;10(1):984–997.
37. Cheng W, Nie J, Xu L, et al. pH-sensitive delivery vehicle based on folic acid-conjugated polydopamine-modified mesoporous silica nanoparticles for targeted cancer therapy. *ACS Appl Mater Interfaces*. 2017; 9(22):18462–18473.
38. Ding X, Liu J, Li J, et al. Polydopamine coated manganese oxide nanoparticles with ultrahigh relaxivity as nanotheranostic agents for magnetic resonance imaging guided synergetic chemo-/photothermal therapy. *Chem Sci*. 2016;7(11):6695–6700.
39. Miao ZH, Wang H, Yang H, Li ZL, Zhen L, Xu CY. Intrinsically Mn^{2+}-chelated polydopamine nanoparticles for simultaneous magnetic resonance imaging and photothermal ablation of cancer cells. *ACS Appl Mater Interfaces*. 2015;7(31):16946–16952.
40. Wei Y, Gao L, Wang L, et al. Polydopamine and peptide decorated doxorubicin-loaded mesoporous silica nanoparticles as a targeted drug delivery system for bladder cancer therapy. *Drug Deliv*. 2017;24(1): 681–691.
41. Cui J, Yan Y, Such GK, et al. Immobilization and intracellular delivery of an anticancer drug using mussel-inspired polydopamine capsules. *Biomacromolecules*. 2012;13(8):2225–2228.
42. Hong D, Lee H, Kim BJ, et al. A degradable polydopamine coating based on disulfide-exchange reaction. *Nanoscale*. 2015;7(47):20149–20154.
43. Muhammad F, Wang A, Qi W, Zhang S, Zhu G. Intracellular antioxidants dissolve man-made antioxidant nanoparticles: using redox vulnerability of nanoceria to develop a responsive drug delivery system. *ACS Appl Mater Interfaces*. 2014;6(21):19424–19433.
44. Asati A, Kaittanis C, Santra S, Perez JM. pH-tunable oxidase-like activity of cerium oxide nanoparticles achieving sensitive fluorigenic detection of cancer biomarkers at neutral pH. *Anal Chem*. 2011;83(7): 2547–2553.
45. Asati A, Santra S, Kaittanis C, Nath S, Perez JM. Oxidase-like activity of polymer-coated cerium oxide nanoparticles. *Angew Chem Int Ed Engl*. 2009;48(13):2308–2312.
46. Mandoli C, Pagliari F, Pagliari S, et al. Stem cell aligned growth induced by CeO_2 nanoparticles in plga scaffolds with improved bioactivity for regenerative medicine. *Adv Funct Mater*. 2010;20(10):1617–1624.
47. Gao W, Wei X, Wang X, Cui G, Liu Z, Tang B. A competitive coordination-based CeO_2 nanowire-DNA nanosensor: fast and selective detection of hydrogen peroxide in living cells and in vivo. *Chem Commun*. 2016;52(18):3643–3646.
48. Kwon HJ, Cha MY, Kim D, et al. Mitochondria-targeting ceria nanoparticles as antioxidants for Alzheimer's Disease. *ACS Nano*. 2016;10(2): 2860–2870.
49. Xiang J, Li J, He J, et al. Cerium oxide nanoparticle modified scaffold interface enhances vascularization of bone grafts by activating calcium channel of mesenchymal stem cells. *ACS Appl Mater Interfaces*. 2016; 8(7):4489–4499.
50. Yang L, Ren Y, Pan W, et al. Fluorescent nanocomposite for visualizing cross-talk between microRNA-21 and hydrogen peroxide in ischemia-reperfusion injury in live cells and in vivo. *Anal Chem*. 2016;88(23): 11886–11891.
51. Park EJ, Choi J, Park YK, Park K. Oxidative stress induced by cerium oxide nanoparticles in cultured BEAS-2B cells. *Toxicology*. 2008; 245(1–2):90–100.
52. Lin W, Huang YW, Zhou XD, Ma Y. Toxicity of cerium oxide nanoparticles in human lung cancer cells. *Int J Toxicol*. 2006;25(6):451–457.
53. Perez JM, Asati A, Nath S, Kaittanis C. Synthesis of biocompatible dextrancoated nanoceria with pH-dependent antioxidant properties. *Small*. 2008;4(5):552–556.
54. Xu C, Qu X. Cerium oxide nanoparticle: a remarkably versatile rare earth nanomaterial for biological applications. *NPG Asia Mater*. 2014; 6(3):e90.
55. Xu C, Lin Y, Wang J, et al. Nanoceria-triggered synergetic drug release based on CeO_2-capped mesoporous silica host-guest interactions and switchable enzymatic activity and cellular effects of CeO_2. *Adv Healthc Mater*. 2013;2(12):1591–1599.
56. Alili L, Sack M, Karakoti A, et al. Combined cytotoxic and anti-invasive properties of redox-active nanoparticles in tumor-stroma interactions. *Biomaterials*. 2011;32(11):2918–2929.
57. Hussain S, Al-Nsour F, Rice AB, et al. Cerium dioxide nanoparticles induce apoptosis and autophagy in human peripheral blood monocytes. *ACS Nano*. 2012;6(7):5820–5829.
58. Gao W, Zhang Z, Li J, Ma Y, Qu Y. Surface engineering on CeO_2 nanorods by chemical redox etching and their enhanced catalytic activity for CO oxidation. *Nanoscale*. 2015;7(27):11686–11691.
59. Kato H, Uzawa H, Nagatsuka T, et al. Preparation and evaluation of lactose-modified monoliths for the adsorption and decontamination of plant toxins and lectins. *Carbohydr Res*. 2011;346(13):1820–1826.
60. Wu J, Zhang J, Deng C, Meng F, Cheng R, Zhong Z. Robust, responsive, and targeted plga anticancer nanomedicines by combination of reductively cleavable surfactant and covalent hyaluronic acid coating. *ACS Appl Mater Interfaces*. 2017;9(4):3985–3994.
61. Shao L, Zhang R, Lu J, Zhao C, Deng X, Wu Y. Mesoporous silica coated polydopamine functionalized reduced graphene oxide for synergistic targeted chemo-photothermal therapy. *ACS Appl Mater Interfaces*. 2017;9(2):1226–1236.

62. Cao S, Pei Z, Xu Y, Pei Y. Glyco-nanovesicles with activatable near-infrared probes for real-time monitoring of drug release and targeted delivery. *Chem Mater*. 2016;28(12):4501–4506.
63. Xu FJ, Kang ET, Neoh KG. pH- and temperature-responsive hydrogels from crosslinked triblock copolymers prepared via consecutive atom transfer radical polymerizations. *Biomaterials*. 2006;27(14):2787–2797.
64. Shao D, Lu MM, Zhao YW, et al. The shape effect of magnetic mesoporous silica nanoparticles on endocytosis, biocompatibility and biodistribution. *Acta Biomater*. 2017;49:531–540.